10.1098/rsta.2003.1335

THE ROYAL SOCIETY

Plane-wave basis finite elements and boundary elements for three-dimensional wave scattering

By E. Perrey-Debain, O. Laghrouche, P. Bettess and J. Trevelyan

School of Engineering, University of Durham, Science Laboratories, South Road, Durham DH1 3LE, UK

Published online 21 January 2004

Classical finite-element and boundary-element formulations for the Helmholtz equation are presented, and their limitations with respect to the number of variables needed to model a wavelength are explained. A new type of approximation for the potential is described in which the usual finite-element and boundary-element shape functions are modified by the inclusion of a set of plane waves, propagating in a range of directions evenly distributed on the unit sphere. Compared with standard piecewise polynomial approximation, the plane-wave basis is shown to give considerable reduction in computational complexity. In practical terms, it is concluded that the frequency for which accurate results can be obtained, using these new techniques, can be up to 60 times higher than that of the conventional finite-element method, and 10 to 15 times higher than that of the conventional boundary-element method.

Keywords: plane waves; finite elements; boundary elements; wave scattering

1. Introduction and statement of the problem

There is considerable interest in many application fields in the solution of the Helmholtz equation when the wavelength is short. There are important applications in electromagnetic scattering (radar cross-sections, electromagnetic compatibility, mobile telephones, etc.), in high-frequency acoustics (aircraft and road-vehicle noise), and geophysics (hydrocarbon exploration), to name but a few. The economic importance of a reliable and computationally efficient solution to such problems is difficult to overstate.

Current finite and boundary-element solutions both suffer from the well-known '10 degrees of freedom per wavelength' requirement if reliable solutions are sought. In many applications, this leads to very large problems and intolerable complexity, so that, even on the largest computers either built or in prospect, there is a limit to the upper frequency that can be considered, which is well below the range of high frequencies of practical interest. There is therefore a significant theoretical impetus to extend finite and boundary-element methods to attack short-wave problems. In the last decade, numerous numerical methods were devised for this purpose (Bettess 2004). Mainly developed for domain-based methods, one direction of particular

One contribution of 13 to a Theme 'Short-wave scattering'.

interest to us is the reduction of the complexity by considering a more elaborate basis to approximate the unknown field. In this regard, Trefftz-type methods involve looking for an approximate solution of a boundary-value problem, from among the sets of functions that satisfy exactly the differential equation, but do not necessarily satisfy the prescribed boundary conditions. Many researchers applied this idea to the Helmholtz problem (Cheung *et al.* 1991; Stojek 1998; Monk & Wang 1999; Farhat *et al.* 2001). In the same vein, the ultraweak variational formulation (UWVF) introduced by Després (1994) and Cessenat & Després (1998) benefits from more solid theoretical foundations and has been recently extended for the inhomogeneous wave equation (Huttunen *et al.* 2002). All these techniques share the same feature that 'inter-element continuity' is not automatically satisfied, and this needs to be enforced by means of appropriate treatments (except maybe for the UWVF, where conformity is ensured in the formulation itself). In the same period, Babuška & Melenk (1997) introduced the partition-of-unity finite-element method (PUFEM). The PUFEM offers an easy way to include analytical information about the problem being solved in a conventional finite-element space. This has the advantage of preserving both *a priori* knowledge about the local behaviour of the solution and conformity. Compared with standard finite elements, the use of the plane-wave basis in the PUFEM has been shown to give significant reduction in computational complexity when solving the Helmholtz equation in two-dimensional domains (Melenk & Babuška 1996; Mayer & Mandel 1997; Laghrouche & Bettess 2000; Ortiz & Sanchez 2001; Laghrouche *et al.* 2002).

By using geometrical optics arguments, the plane-wave basis as introduced in the PUFEM has been investigated theoretically by de La Bourdonnaye (1994*a*, *b*) under the title of 'microlocal discretization' (MD) for solving scattering problems with integral equations. The method was developed further by Perrey-Debain *et al.* (2003*a*, *b*) for bi-dimensional obstacles. In practical terms, the results of their work show that the plane-wave basis enables the supported frequency range to be extended by a factor of 3–4 over conventional boundary elements even for non-convex complex geometries. A particular use of the MD where only the incident plane wave is included in the basis can be found in Abboud *et al.* (1995) and Darrigrand (2002). However, this asymptotic method is restricted to convex obstacles and sufficiently high frequency.

In the present paper, we are dealing with the numerical implementation and efficiency assessment of the plane-wave basis in both finite-element and boundary-element contexts for three-dimensional Helmholtz problems. The delicate question of numerical stability due to conditioning problems of the resulting algebraic system is briefly mentioned and it is believed that these issues merit a separate paper.

The problem under consideration is an exterior acoustic scattering problem. To be precise, we wish to find the field distribution $\Phi = \Phi(\boldsymbol{r})$ in a domain Ω in $\mathbb{R}^3$ exterior to a closed bounded regular surface Γ. For a perfectly reflecting surface, the scalar field Φ satisfies the following problem:

$$\Delta\Phi + \kappa^2\Phi = 0 \quad \text{in } \Omega, \tag{1.1}$$

$$\frac{\partial\Phi}{\partial\boldsymbol{n}} = 0 \quad \text{on } \Gamma, \tag{1.2}$$

$$\lim_{r\to\infty} r\left(\frac{\partial\Phi^{\mathrm{S}}}{\partial r} - \mathrm{i}\kappa\Phi^{\mathrm{S}}\right) = 0, \tag{1.3}$$

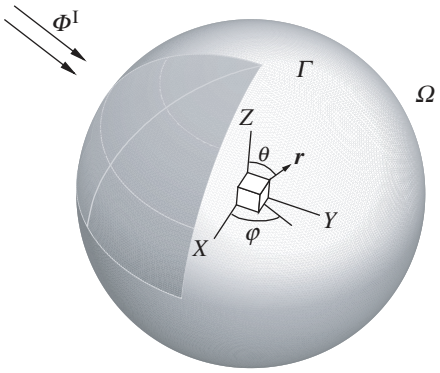

Figure 1. Problem statement and notation. Typical triangular and rectangular patches on the scattering surface are also shown.

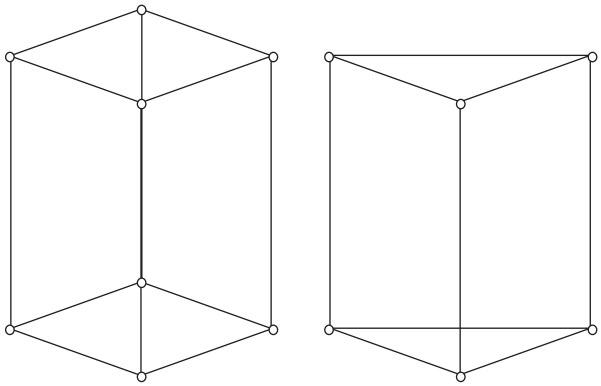

Figure 2. Rectangular- and triangular-type finite elements.

where κ is the wavenumber (so that $\lambda = 2\pi/\kappa$ is the wavelength), $r = |\boldsymbol{r}|$ is the distance between the origin and the position $\boldsymbol{r} = (x, y, z)$, $\boldsymbol{n}$ denotes the outward normal unit vector on the surface Γ, $\Phi^{\mathrm{S}} = \Phi - \Phi^{\mathrm{I}}$ is the scattered field, and Φ^{I} is a prescribed incident plane wave. Variables φ and θ stand for the classical spherical angular coordinates as illustrated in figure 1.

2. Plane-wave basis finite elements

(*a*) *Mathematical Formulation*

The finite-element discretization of the exterior scattering problem can be achieved if the Sommerfeld condition (1.3) is replaced by its approximation on an artificial boundary that delimits a finite computational domain $\Omega' \subset \Omega$. At this boundary, the scattered potential behaves as $\mathrm{e}^{\mathrm{i}\kappa r}/r$ and therefore a simple local form of such an artificial absorbing condition is given by the approximation

$$\frac{\partial \Phi^{\mathrm{S}}}{\partial r} + \frac{\Phi^{\mathrm{S}}}{r} - \mathrm{i}\kappa \Phi^{\mathrm{S}} = 0 \quad \text{on } \Gamma_\infty, \tag{2.1}$$

where the spherical surface Γ_∞ is the outer part of the boundary of Ω'. Whereas more sophisticated boundary conditions can be found in Bayliss *et al.* (1992), the

approximate condition (2.1) has the advantage of being easier to implement and performs well as long as the external boundary is located sufficiently far from the scatterer. A standard weighted residual scheme is applied to the Helmholtz equation, so the inner product (we took the scattered potential as the unknown for pure convenience)

$$\int_{\Omega'} W(\Delta \Phi^{\mathrm{S}} + \kappa^2 \Phi^{\mathrm{S}})\,\mathrm{d}\Omega' = 0, \tag{2.2}$$

where W is a properly chosen weighting function, gives the governing integral equation for the problem. Applying Green's first theorem with (1.2) and (2.1), the problem is formulated in a weak form as

$$B(W, \Phi^{\mathrm{S}}) = \int_{\Gamma} W \frac{\partial \Phi^{\mathrm{I}}}{\partial \boldsymbol{n}}\,\mathrm{d}\Gamma, \tag{2.3}$$

where B denotes the bilinear form

$$B(W, \Phi^{\mathrm{S}}) = \int_{\Omega'} (\nabla W \cdot \nabla \Phi^{\mathrm{S}} - \kappa^2 W \Phi^{\mathrm{S}})\,\mathrm{d}\Omega' + \int_{\Gamma_\infty} W\left(\frac{1}{r} - \mathrm{i}\kappa\right)\Phi^{\mathrm{S}}\,\mathrm{d}\Gamma_\infty. \tag{2.4}$$

Let the domain Ω' be partitioned into K non-overlapping subdomains Ω^k, $k = 1, \ldots, K$. Each subdomain, or finite element in the engineering terminology, is given through a coordinate transformation $\boldsymbol{r} = L^k(\boldsymbol{\eta})$ between the real space and the local system $\boldsymbol{\eta} = (\eta_1, \eta_2, \eta_3) \in \mathcal{L}$. As illustrated in figure 2, they can be either of rectangular type with $\mathcal{L} = [-1, 1]^3$ or of triangular type with $\mathcal{L} = \mathcal{T} \times [-1, 1]$, where $\mathcal{T}$ denotes the triangular domain

$$\mathcal{T} = \{\eta_1 \geqslant 0,\ \eta_2 \geqslant 0,\ \eta_1 + \eta_2 \leqslant 1\}. \tag{2.5}$$

Using a conventional piecewise linear finite-element space, the quantity Φ^{S} on Ω^k is approximated as

$$\Phi^{\mathrm{S}} = \sum_{p=1}^{\#\mathrm{vert}} N_p(\boldsymbol{\eta})\Phi_p, \quad \#\mathrm{vert} = 6 \text{ or } 8, \tag{2.6}$$

where N_p denotes the (P_1) Lagrangian polynomial on $\mathcal{L}$ and Φ_p are the nodal values corresponding to the vertices of $\mathcal{L}$ (#vert = 6 for the triangular type and #vert = 8 for the rectangular type). The linear approximation (2.6) requires the mesh size to be of order $\lambda/10$ and suffers from the so-called 'dispersion and pollution effects' for high wavenumbers (Ihlenburg & Babuška 1995, 1997). These limitations can be alleviated if a set of plane waves travelling in multiple directions is also included. Following Babuška & Melenk (1997), the new plane-wave approximation reads

$$\Phi^{\mathrm{S}} = \sum_{p=1}^{\#\mathrm{vert}} N_p(\boldsymbol{\eta}) \sum_{q=1}^{Q_p} \exp(\mathrm{i}\kappa \boldsymbol{\xi}_p^q \cdot \boldsymbol{r})\Phi_p^q, \tag{2.7}$$

where the point $\boldsymbol{r}$ describes the subdomain Ω^k. Coefficients Φ_p^q no longer represent the nodal values, but are now the amplitudes of the set of Q_p plane waves associated with each vertex p. If two subdomains share a common vertex, then the associated set of directions and amplitudes are identical. This guarantees the continuity of the

potential all over the computational domain Ω'. The plane-wave directions may be distributed evenly on the unit sphere, but may also be irregularly distributed if, for example, some knowledge about a prevailing wave direction is available. We leave this last point for further studies and, in this paper, directions $\boldsymbol{\xi}_p^q$ are built by discretizing uniformly the surface of the cube $[-1,1]^3$ by points $\boldsymbol{u}_q$, $q = 1, \ldots, Q_p$; unit vectors are then simply obtained by $\boldsymbol{\xi}_p^q = \boldsymbol{u}_q/|\boldsymbol{u}_q|$.

(*b*) *Implementation and results*

In this work, a Galerkin scheme is used so that the test function W is chosen from the plane-wave basis functions (2.7). This choice leaves us with the numerical evaluation of oscillatory functions to be integrated over multi-wavelength sized elements. They are of the form

$$\int_{\Omega^k} f(\boldsymbol{\eta}) \exp(\mathrm{i}\kappa(\boldsymbol{\xi}_p^q + \boldsymbol{\xi}_{p'}^{q'}) \cdot \boldsymbol{r}) \, \mathrm{d}\Omega^k, \tag{2.8}$$

where $f(\boldsymbol{\eta})$ is a 'slow' varying function and a prime refers to the test function. Special integration rules were developed to integrate such forms in two dimensions for some simple geometry finite elements (Ortiz & Sanchez 2001; Bettess *et al.* 2003). In this paper, high-order Gauss–Legendre integration schemes are used. Integrals over rectangular subdomains are computed in a straightforward manner using one-dimensional integration formulae over the interval $[-1,1]$. Integration over the triangular domain $\mathcal{T}$ is carried out by general Cartesian product rules (Krommer & Ueberhuber 1998) as

$$\int_0^1 \int_0^{\eta_0} F(\eta_1, \eta_0) \, \mathrm{d}\eta_1 \, \mathrm{d}\eta_0 \approx \sum_{i=1}^{n_0} c_i^{(n_0)} t_i^{(n_0)} \sum_{j=1}^{n_{1,i}} c_j^{(n_{1,i})} F(t_i^{(n_0)} t_j^{(n_{1,i})}, t_i^{(n_0)}), \tag{2.9}$$

where $\eta_0 = \eta_1 + \eta_2$ and F is the quantity to be integrated. The set

$$\{c_i^{(n)};\ t_i^{(n)};\ i = 1, \ldots, n\}$$

stands for the classical quadrature weights and abscissae of the n-point Gauss–Legendre formula on the interval $[0,1]$. In order to get a homogeneous distribution of the integration points, $n_{1,i}$ is taken to be linearly varying with the η_0-coordinate as $n_{1,i} = \lfloor \alpha n_0 t_i^{(n_0)} \rfloor + \beta$. In practice, $\alpha = 1$ and $\beta = 10$ have been found to be adequate, though other choices are possible.

To assess the accuracy of the method, we consider the case of an incident plane wave impinging on a rigid sphere of unit radius. This problem has an analytical solution that can be found in standard textbooks such as Morse & Feshbach (1953). Now, let R be the radius of the outer surface Γ_∞ and $\Omega' = \{\boldsymbol{r} \text{ such that } 1 \leqslant |\boldsymbol{r}| \leqslant R\}$ be the computational domain. Numerical errors due to some geometrical approximation can be avoided if subdomains are built so that they exactly describe the scattering and outer surfaces. This can be performed by first partitioning the unit sphere with I longitude lines and J latitude lines as illustrated in figure 1. Rectangular patches are given by the spherical angles (θ, φ) via linear interpolation

$$\theta = \tfrac{1}{2}(1 + \eta_2)\frac{\pi}{J+1} + \theta^0, \qquad \varphi = (1 + \eta_1)\frac{\pi}{I} + \varphi^0, \tag{2.10}$$

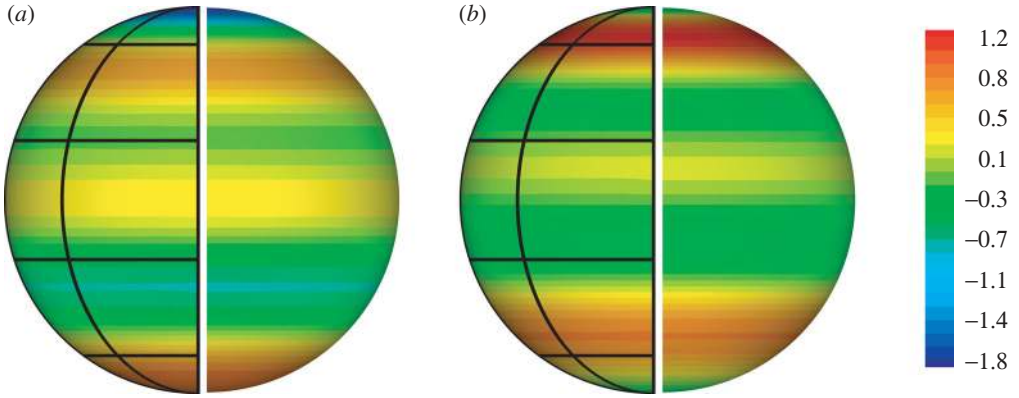

Figure 3. Scattered potential around the sphere, $\kappa = 2\pi$: (a) real part, (b) imaginary part.

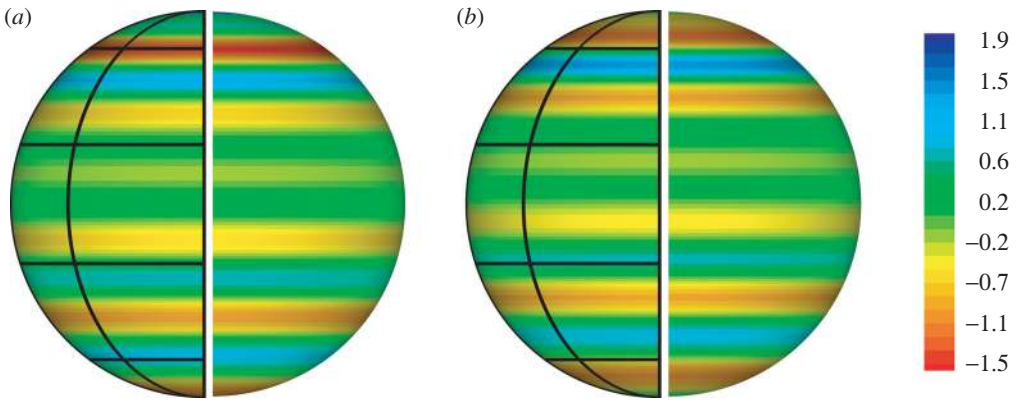

Figure 4. Scattered potential around the sphere, $\kappa = 5\pi$: (a) real part, (b) imaginary part.

where θ^0 and φ^0 are constants depending on the patch location. However, around the poles, triangular-type patches must be used and spherical angles are given by the following transformation (this example refers to the north pole):

$$\theta = (\eta_1 + \eta_2)\frac{\pi}{J+1} \quad \text{and} \quad \varphi = \left(\frac{\eta_1}{\eta_1 + \eta_2}\right)\frac{2\pi}{I} + \varphi^0. \tag{2.11}$$

The partitioning of Ω' is finally achieved by subdividing the interval $[1, R]$ into L equal sized intervals over each of which the radius is obtained via linear interpolation. This operation leads to $I \times (J+1) \times L$ subdomains with $(I \times J+2) \times (L+1)$ vertices.

In the following applications, Ω' is partitioned with a constant number of subdomains with $I = 8$ longitude lines, $J = 4$ latitude lines and $L = 4$ layers. Thus, a total of 160 finite elements with 170 vertices form the mesh. The outer surface is taken four wavelengths distant from the scatterer (previous numerical tests show that this is a sufficient distance for applying the radiation condition (2.1)). The number of plane waves attached to each vertex is constant and is therefore referred to by a single number, Q. The total number of variables needed to represent the scattered field in the computational domain is then simply given by $N = 170Q$ and we can

Table 1. *Plane-wave scattering by a unit sphere*

test	κ	Q	N	ε_2	τ
1	π	58	9 860	0.1%	2.95
2	2π	58	9 860	0.8%	2.66
3	3π	58	9 860	2.1%	2.43
4	4π	98	16 660	0.9%	2.67
5	5π	98	16 660	2.7%	2.48

define the number of degrees of freedom per wavelength τ by

$$\tau = \lambda \left(\frac{N}{\mathrm{vol}(\Omega')} \right)^{1/3}, \tag{2.12}$$

where $\mathrm{vol}(\Omega')$ is the volume of Ω'. The accuracy of the model is measured by the relative $L_2(\Gamma)$-norm error defined by

$$\varepsilon_2 = \frac{\|\Phi^{\mathrm{S}} - \tilde{\Phi}^{\mathrm{S}}\|_{L^2(\Gamma)}}{\|\tilde{\Phi}^{\mathrm{S}}\|_{L^2(\Gamma)}}, \tag{2.13}$$

where Φ^{S} and $\tilde{\Phi}^{\mathrm{S}}$ denote the computed and exact scattered fields, respectively.

Performances of the method are conveniently summarized in table 1. As is clearly shown, a discretization level of about 2.5 variables per wavelength is sufficient to achieve *ca.* 1% of error. Results can even improve by an order of magnitude by simply taking around three variables per wavelength. This is in agreement with the approximation properties of the plane-wave basis when solving the Helmholtz equation (Babuška & Melenk 1997). However, it has been observed that results can quickly deteriorate if τ is taken below 2.5. This suggests that the asymptotic complexity is still behaving as $\mathcal{O}(\kappa^3)$ as for the conventional FEM. In practical terms, this new finite-element basis enables the compression of the information by a factor of $3^3 \approx 30$ to $4^3 \approx 60$ over conventional finite elements. These estimations are obviously subject to variations depending on the problem. Figures 3 and 4 show the scattered potential on the surface of the sphere for $\kappa = 2\pi$ and $\kappa = 5\pi$. Numerical results are reported on the meshed half sphere and analytical solutions are reported on the other half. Both figures show very good agreement and discrepancies are too small to be seen. At this stage, it is believed that significant storage improvements can still be achieved if more sophisticated non-reflecting conditions are incorporated to reduce the size of the computational domain. Speeding up the numerical evaluation of element matrices is another challenging issue which needs to be considered in the near future.

3. Plane-wave basis boundary elements

(*a*) *Mathematical formulation*

The integration by parts (2.3) leads to the need to discretize the propagative medium Ω and requires truncation of the infinite region. By choosing W as the fundamental solution of the Helmholtz equation satisfying the radiation condition (1.3), i.e. the

free-space Green function,

$$G(\boldsymbol{r},\boldsymbol{r}') = \frac{\exp(\mathrm{i}\kappa|\boldsymbol{r}-\boldsymbol{r}'|)}{4\pi|\boldsymbol{r}-\boldsymbol{r}'|}, \tag{3.1}$$

and, applying Green's second identity, we arrive at the well-known Helmholtz integral equation formulation

$$\Phi(\boldsymbol{r}) - (\mathcal{K}\Phi)(\boldsymbol{r}) = 2\Phi^{\mathrm{I}}(\boldsymbol{r}), \quad \boldsymbol{r}\in\Gamma, \tag{3.2}$$

where

$$(\mathcal{K}\Phi)(\boldsymbol{r}) = 2\int_{\Gamma} \frac{\partial G(\boldsymbol{r},\boldsymbol{r}')}{\partial \boldsymbol{n}(\boldsymbol{r}')}\Phi(\boldsymbol{r}')\,\mathrm{d}\Gamma(\boldsymbol{r}') \tag{3.3}$$

denotes the double-layer potential.

To solve (3.2), the strategy is very similar to the finite-element procedure of the previous section. The distinctive features here are that only the discretization of the scattering surface is needed and the integration of the singularity of the test function has to be handled properly. The scattering surface Γ is described by a number, K, of non-overlapping patches Γ^k, $k=1,\ldots,K$, such that Γ^k is the image of the coordinate set $\mathcal{T}$ (2.5) via the regular parametrization

$$\boldsymbol{r} = T^k(\eta_1,\eta_2) \quad \text{with } (\eta_1,\eta_2)\in\mathcal{T}. \tag{3.4}$$

The unknown field is approximated over the patch Γ^k by a 'surface' plane-wave-basis finite element as

$$\Phi = \sum_{p=1}^{3} N_p(\eta_1,\eta_2)\sum_{q=1}^{Q_p}\exp(\mathrm{i}\kappa\boldsymbol{\xi}_p^q\cdot\boldsymbol{r})\Phi_p^q, \tag{3.5}$$

where the point $\boldsymbol{r}$ describes the surface Γ^k and N_p denotes the (P_1) Lagrangian polynomial on $\mathcal{T}$. Directions $\boldsymbol{\xi}_p^q$ are chosen so that they are regularly distributed on the unit sphere (see § 2 *a*). If two patches share a common vertex, then the associated set of directions and amplitudes are identical. Thus, Φ is piecewise C^∞ and globally C^0 on Γ.

(*b*) *Element matrices and integration algorithm*

The collocation method has been found to produce very accurate results for bi-dimensional obstacles of smooth boundary line (Perrey-Debain *et al*. 2003*a*, *b*). Moreover, it has the advantage of being easier to implement and leads to faster integration procedures than a Galerkin scheme. The same technique will be used here. Let M points $\boldsymbol{r}_i$, $i=1,\ldots,M$, be evenly distributed over the scattering surface. Writing (3.2) at those points yields the following system

$$\boldsymbol{A\Phi} = (\boldsymbol{W}-\boldsymbol{K})\boldsymbol{\Phi} = \boldsymbol{b}, \tag{3.6}$$

where the vector $\boldsymbol{\Phi}$ contains the plane-wave coefficients. The sparse matrix $\boldsymbol{W}$ can be interpreted as a plane-wave interpolation matrix, $\boldsymbol{K}$ is the boundary-element matrix stemming from the integral of (3.2) and $\boldsymbol{b}$ is the source vector containing the incident field. The non invertibility of the integral operator (3.2) when κ is an eigenfrequency

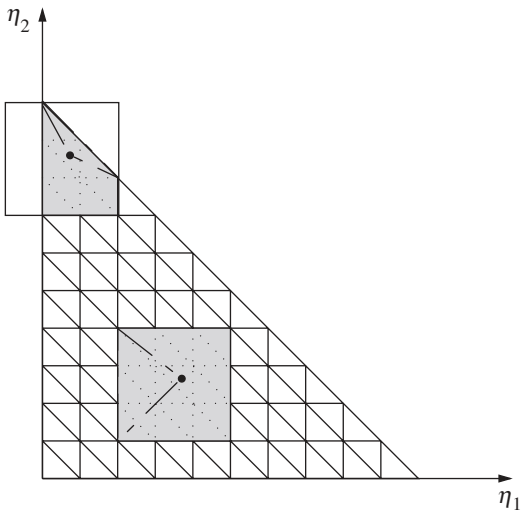

Figure 5. Integration scheme over $\mathcal{T}$ with $m = 10$. The singular integration is performed over a polygon domain (grey-coloured region) in the vicinity of the collocation point (black circles).

Table 2. *Regular integration algorithm*

do for $k \in \{1, \ldots, K\}$

Regular integration for $\boldsymbol{r}_i \notin \Gamma^k$

do for all $\boldsymbol{r}' \in T^k\{\mathrm{GCPR}\}$
compute geometrical information at $\boldsymbol{r}'$
compute and store plane-wave bases at $\boldsymbol{r}'$
do for all $\boldsymbol{r}_i \notin \Gamma^k$
compute kernel $\boldsymbol{g}(\boldsymbol{r}_i, \boldsymbol{r}')$
update element matrices
end do
end do

Regular integration for $\boldsymbol{r}_i \in \Gamma^k$

do for all $\boldsymbol{r}' \in T^k\{\mathrm{LJ}\}$
compute geometrical information at $\boldsymbol{r}'$
compute and store plane-wave bases at $\boldsymbol{r}'$
do for all $\boldsymbol{r}_i \in \Gamma^k$
if $\boldsymbol{r}' \notin T^k\{\mathcal{S}(\boldsymbol{r}_i)\}$
compute kernel $\boldsymbol{g}(\boldsymbol{r}_i, \boldsymbol{r}')$
update element matrices
end if
end do
end do

end do

of the corresponding interior Dirichlet problem is alleviated by completing the system (3.6) with M^0 additional constraints (Schenck 1968)

$$(\mathcal{K}\Phi)(\boldsymbol{r}_i^0) = -2\Phi^{\mathrm{I}}(\boldsymbol{r}_i^0), \quad i = 1, \ldots, M^0, \tag{3.7}$$

where the points $\boldsymbol{r}_i^0$ are taken to be *inside* the scattering obstacle.

The computation of the boundary matrix $\boldsymbol{K}$ is expected to be prohibitively long at high frequency, since we need to integrate oscillatory functions over two-dimensional patches of many wavelengths in extent with sufficient accuracy. Thus, the use of the stationary phase to accelerate the calculation was suggested (Abboud *et al.* 1995). More recently, Darrigrand (2002) applied the fast multipole method for the same purpose. In our work, classical quadrature rules have been employed. Typical integrals over Γ^k are of the form

$$\int_{\mathcal{T}} \boldsymbol{g}(\boldsymbol{r}_i, \boldsymbol{r}') \cdot \left(\frac{\partial \boldsymbol{r}'}{\partial \eta_1} \times \frac{\partial \boldsymbol{r}'}{\partial \eta_2} \right) N_p(\eta_1, \eta_2) \exp(\mathrm{i}\kappa \boldsymbol{\xi}_p^q \cdot \boldsymbol{r}') \, \mathrm{d}\eta_1 \, \mathrm{d}\eta_2, \tag{3.8}$$

where $\boldsymbol{r}' = T^k(\eta_1, \eta_2)$ and the $\boldsymbol{r}_i$-dependent kernel $\boldsymbol{g}(\boldsymbol{r}_i, \boldsymbol{r}')$ is given by

$$\boldsymbol{g}(\boldsymbol{r}_i, \boldsymbol{r}') = \frac{\exp(\mathrm{i}\kappa|\boldsymbol{r}_i - \boldsymbol{r}'|)}{4\pi|\boldsymbol{r}_i - \boldsymbol{r}'|^3} (\mathrm{i}\kappa|\boldsymbol{r}_i - \boldsymbol{r}'| - 1)(\boldsymbol{r}_i - \boldsymbol{r}'). \tag{3.9}$$

Regular integrals ($\boldsymbol{r}_i \notin \Gamma^k$) are computed with general Cartesian product rules (Krommer & Ueberhuber 1998) such that the distribution of integration points is homogeneous over $\mathcal{T}$ (see (2.9)). In the following 'GCPR' denotes the set of those points. To deal with singular integrals, we split the integration domain into m^2 triangles $\mathcal{T}_n$ of equal size as illustrated in figure 5,

$$\mathcal{T} = \bigcup_{n=1}^{m^2} \mathcal{T}_n. \tag{3.10}$$

Given the parametric coordinates of a collocation point $\boldsymbol{r}_i$, a square domain $\mathcal{S}(\boldsymbol{r}_i)$ of side-length $3/m$ surrounding the singular point is defined. The planar polygon $\mathcal{P}(\boldsymbol{r}_i) = \mathcal{S}(\boldsymbol{r}_i) \cap \mathcal{T}$ is split up into a finite number of triangles with the singular point as a common vertex. Each of these triangles is mapped onto the reference domain $\mathcal{T}$ with the singularity at the origin. Then, using the nonlinear transformation (Duffy 1982),

$$\eta_1 = \bar{\eta}_1 \quad \text{and} \quad \eta_2 = \bar{\eta}_1 \bar{\eta}_2, \tag{3.11}$$

the singularity is removed and the integration is performed with standard quadrature rules. For collocation points belonging to more than one patch (i.e. edges or vertices), the integration is performed in the same manner over each patch involved.

The regular integration over the other triangles is carried out with a 19-point formula (Lyness & Jespersen 1975) and we call 'LJ' the set of all those points in $\mathcal{T}$ (note $\#\mathrm{LJ} = 19m^2$). To avoid recomputing the same information (geometry and plane-wave bases) independent of the collocation point, the code has been written in the spirit of the Reusable Intrinsic Sample Point (RISP) algorithm (Kane 1994). The regular integration scheme is sketched in table 2. If we fix the number of patches K whatever the frequency, we arrive at the classical estimation that $\#\mathrm{GCPR} \sim \kappa^2$ and also $\#\mathrm{LJ} \sim \kappa^2$. Therefore, the size of the singular integration domain decreases as κ^{-1} and singular integrals are computed using a constant number of integration points. The RISP algorithm is thus optimized.

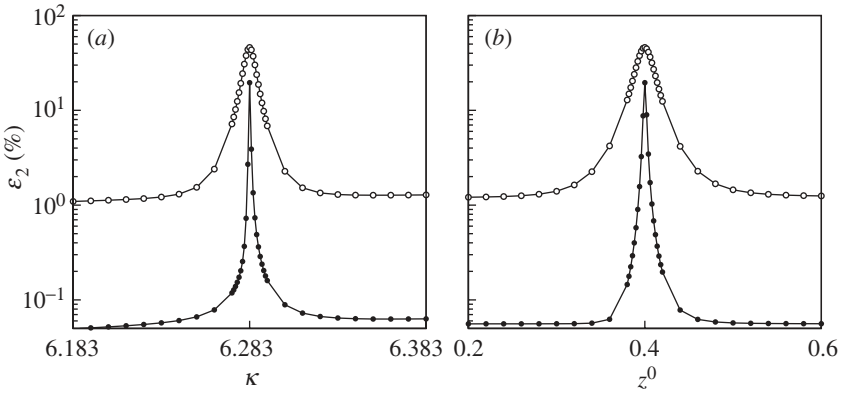

Figure 6. Solution error as a function of (*a*) the frequency (no internal point); (*b*) the z^0 coordinate of one internal point ($\kappa = 2\pi$). Empty circles, $Q = 26$ ($N = 156$); black circles, $Q = 58$ ($N = 348$).

(*c*) *Results*

We consider scatterers given by the spherical parametrization:

$$\boldsymbol{r} = \begin{pmatrix} R_1\varrho(\theta,\varphi)\sin\theta\cos\varphi \\ R_2\varrho(\theta,\varphi)\sin\theta\sin\varphi \\ R_3\varrho(\theta,\varphi)\cos\theta \end{pmatrix}, \quad \theta \in [0,\pi], \quad \varphi \in [0,2\pi], \tag{3.12}$$

where $\varrho(\theta,\varphi)$ is a smooth admissible positive function on $[0,\pi]\times[0,2\pi]$. Eight triangular patches are sufficient to describe the scatterer. For example, the patch corresponding to the first octant $(\theta,\varphi) \in [0,\pi/2]^2$ is obtained via

$$\theta = (\eta_1+\eta_2)\tfrac{1}{2}\pi \quad \text{and} \quad \varphi = \left(\frac{\eta_1}{\eta_1+\eta_2}\right)\frac{\pi}{2}, \quad (\eta_1,\eta_2) \in \mathcal{T}. \tag{3.13}$$

We first compare our results with analytical solutions for the particular case of a vertical plane wave impinging upon a unit sphere. In all cases, the number of directions associated with each vertex is the same and is therefore referred to by a single number Q. Moreover, the incident plane wave is always included in the set. We call N the total number of variables (here, it is simply given by $N = 6Q$). The number of collocation points is chosen such that numerical results have stabilized and in all our applications we considered $M \sim 1.5N$. The exact position of these points is not of crucial importance as long as they are evenly distributed on the scatterer. In our current algorithm, this is done by considering a uniform distribution on $\mathcal{T}$. Obviously, in case of severe distortions in the mapping (3.4), this distribution might be rearranged to ensure uniformity in the real space. This is the subject of further investigation, and such situations will not be considered in the following discussion. Finally, the over-determined system is solved by a standard QR decomposition algorithm for double-precision complex data.

Figure 6*a* shows the effects of the irregular frequency $\kappa = 2\pi$ (note that ε_2 is defined by (2.13)). In the absence of internal points, the solution is masked by the internal mode and it deteriorates in a certain bandwidth centred at the resonance. As expected, the bandwidth narrows with the quality of the approximation. The position

Table 3. *Scattering by a unit sphere (calculations performed on a* 2 GHz *PIV)*

test	κ	Q	N	ε_2	τ	CPU time (QR solver)
1	5	98	588	0.00015%	8.6	18 min 13 s (4 s)
2	10	98	588	0.013%	4.3	4 min 20 s (4 s)
3	15	98	588	1.5%	2.85	5 min 10 s (4 s)
4	20	98	588	12.8%	2.15	5 min 10 s (4 s)
5	20	154	924	0.85%	2.7	13 min 20 s (16 s)
6	30	298	1788	0.95%	2.5	1 h 53 min (2 min)
7	40	490	2940	1.15%	2.4	7 h 18 min (8 min)

of a single internal point located at $(0, 0, z^0)$ is crucial, as shown in figure 6*b*. The solution deteriorates in the neighbourhood of the nodal surface $|\boldsymbol{r}| = \frac{1}{2}$, for which the equation (3.7) is trivial and therefore does not provide a linearly independent constraint. Since internal mode shapes are not known *a priori*, the use of multiple internal points is strongly advised. Note that the additional cost is negligible and does not penalize the method.

Table 3 shows the performance of the method for various configurations. Here τ denotes the number of degrees of freedom per wavelength,

$$\tau = \lambda \left(\frac{N}{\mathrm{ar}(\Gamma)} \right)^{1/2}, \tag{3.14}$$

where $\mathrm{ar}(\Gamma)$ is the area of Γ. Solution errors are strongly dependent on this variable, as indicated in the first four rows, since doubling τ improves the quality of the solution by a factor of 100. As far as the authors are aware, only a p-version boundary-element method could possibly exhibit similar behaviour (Grannell *et al*. 1994). The last two tests show the efficiency of the plane-wave basis since only 2.5 degrees of freedom are sufficient to get reasonable results. Numerous numerical experiments (not shown here) clearly show that, below this threshold, solution quality deteriorates quickly and this behaviour has already been observed in the bi-dimensional case. This confirms that this method still requires $\mathcal{O}(\kappa^2)$ degrees of freedom on the scattering surface as in the conventional boundary-element method (de La Bourdonnaye 1994*a*, *b*) and the gain lies in the proportionality constant. Assuming that 10 variables per wavelength are required to get *ca.* 1% of error if the linear approximation (2.6) is used, the gain is $4^2 = 16$. This permits the study of relatively high-frequency three-dimensional problems on a personal computer.

The major drawback is the CPU time consumed for the matrix evaluation (in brackets are shown computational times for the QR solver). Indeed, if the number of patches is fixed, our method requires $\mathcal{O}(\kappa^6)$ multiplications instead of $\mathcal{O}(\kappa^4)$ in the classical approach. Note that computational times for both regular and singular integrations are slightly overestimated in order to ensure that errors obtained have stabilized. In this regard, two important issues need to be mentioned.

(i) The plane-wave basis can produce very accurate results by simply taking more unknowns per wavelength, for instance $\tau > 4$ is more than sufficient; however,

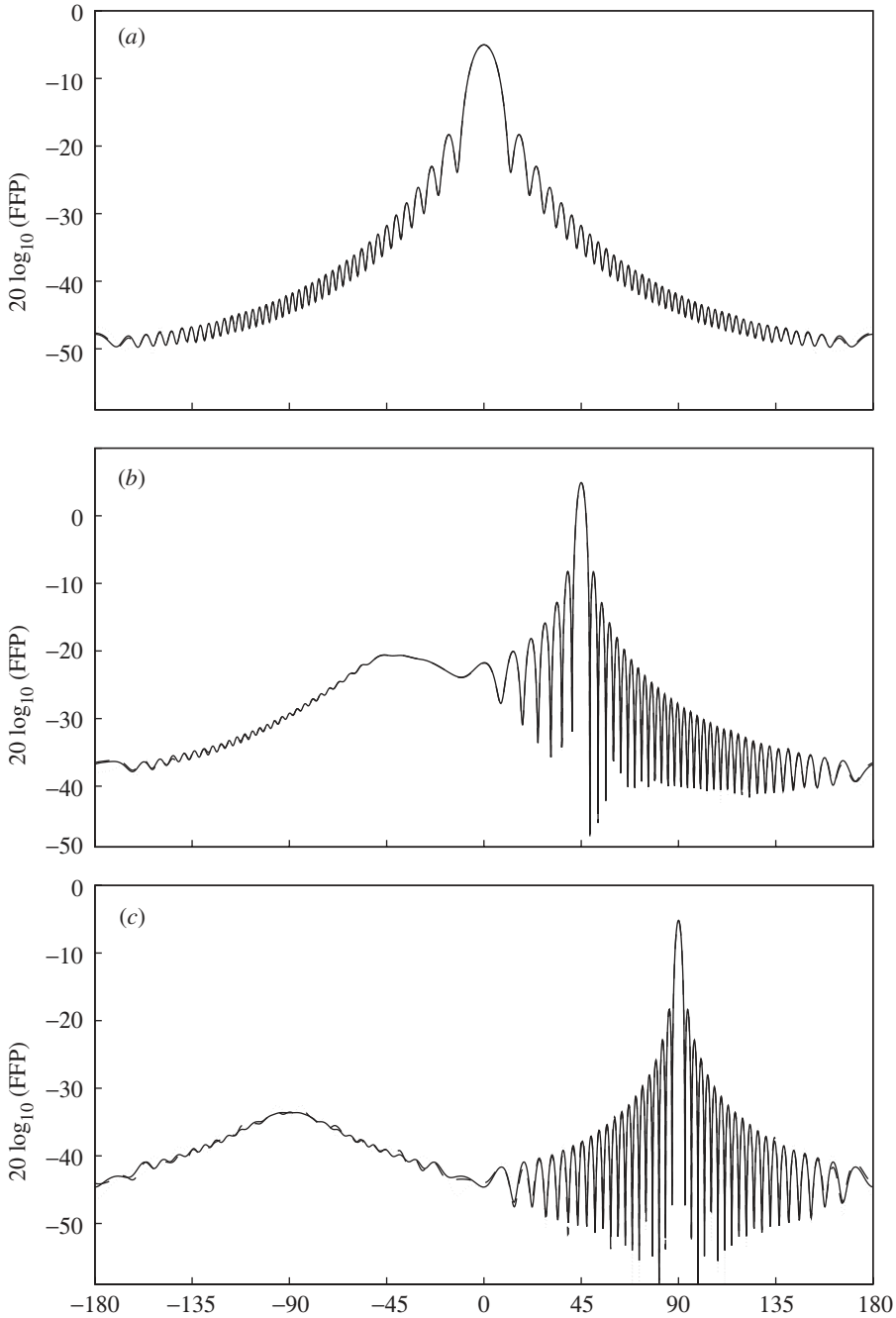

Figure 7. Scattering by an ellipsoid. FFP (in dB) computed in the plane $\varphi = 0$ for three incident plane waves of direction: (*a*) $(0, 0, 1)$; (*b*) $(\sqrt{2}, 0, \sqrt{2})/2$ and (*c*) $(1, 0, 0)$. Dotted line, $N = 930$ ($\tau = 2.25$); dashed line, $N = 1056$ ($\tau = 2.4$); straight line, $N = 1308$ ($\tau = 2.65$).

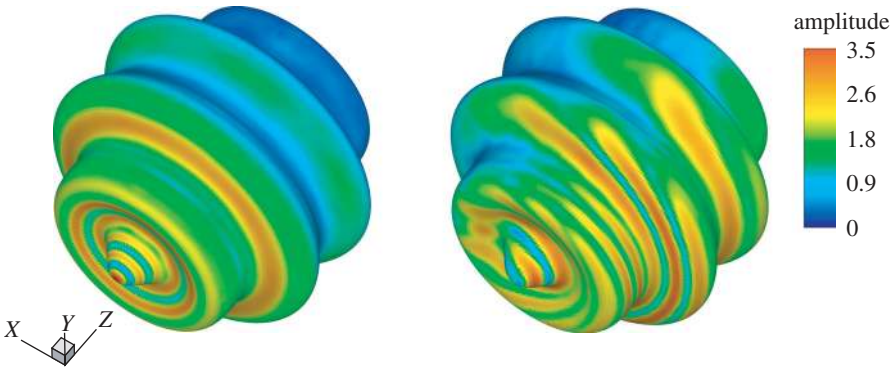

Figure 8. Scattering by a non-convex obstacle at $\kappa = 30$. Isovalues of the field amplitude are shown for two incident plane waves of direction (*a*) (0,0,1) and (*b*) $(\sqrt{2}, 0, \sqrt{2})/2$.

the price to pay is a time consuming integration procedure which is penalizing at high frequency.

(ii) In those configurations (high values for Q and τ), the system matrix is likely to be highly ill-conditioned and singular-value decomposition with truncation of the smallest singular values is advised in order to cancel round-off errors that may mask the high-order accuracy of the method.

Obviously, these matters deserve amelioration. In the following applications, we will assume that we are not facing those situations and only the QR decomposition will be used.

The specific feature of this new method, in contrast with iterative algorithms, is the possibility of storing the QR factorization of $\boldsymbol{A}$ once and for all and using it as a 'black box', whatever the incident field. Even though best performance is obtained when the incident field is chosen in the plane-wave basis set, spherical fields can be handled as long as the source is not too close to the scatterer (Perrey-Debain *et al*. 2003*c*). In the following example, we consider a rigid ellipsoid of size (in wavelengths λ) $3.8 \times 3.8 \times 19.1$ (which corresponds to taking $R_1 = R_2 = \frac{1}{5}$ and $R_3 = \varrho = 1$ at $\kappa = 60$) and three incident plane waves in respective directions $(0, 0, 1)$, $(\sqrt{2}, 0, \sqrt{2})/2$ and $(1, 0, 0)$. We are concerned with the far-field pattern (FFP) defined by (up to a multiplicative constant)

$$\mathrm{FFP}(\hat{\boldsymbol{r}}) = \left| \int_{\Gamma} \hat{\boldsymbol{r}} \cdot \boldsymbol{n}(\boldsymbol{r}') \exp\left(-\mathrm{i}\kappa \hat{\boldsymbol{r}} \cdot \boldsymbol{r}'\right) \Phi(\boldsymbol{r}') \, \mathrm{d}\Gamma(\boldsymbol{r}') \right|, \tag{3.15}$$

where direction $\hat{\boldsymbol{r}}$ describes the unit sphere. Figure 7 shows the FFP (in dB) in the plane $\varphi = 0$ for three numerical configurations:

(i) $Q = 155$ directions at all vertices, which corresponds to a discretization level $\tau = 2.25$;

(ii) $Q = 218$ directions at the poles and $Q = 155$ elsewhere ($\tau = 2.4$); and

(iii) $Q = 218$ directions at all vertices ($\tau = 2.65$).

In all cases, the three incident plane waves are always included in the plane-wave basis. As is clearly shown, 930 degrees of freedom are sufficient to get reasonable results and, with 1056 variables, results have almost reached convergence.

Our final application concerns the scattering of the three previous incident plane waves at $\kappa = 30$ by a non-convex scatterer described by the sinusoidally varying function

$$\varrho(\theta, \varphi) = 1 + \cos(10\theta)/10, \tag{3.16}$$

with $R_1 = R_2 = R_3 = 1$. By choosing $Q = 491$ directions at each vertex (2946 variables), results have been found to be of 'engineering accuracy' (i.e. when changes in the isovalues plot become hardly noticeable). Isovalues of the field amplitude $|\Phi|$ are shown for two incident waves in figure 8. This test corresponds to a discretization level $\tau = 2.9$. The efficiency is not as high as for the sphere, which could be considered as the optimal case. However, the gain is still remarkable here, and the use of conventional boundary elements would require at least 10 times more variables to achieve the same accuracy.

4. Conclusion

This paper has demonstrated the applicability of the plane-wave basis in both finite-element and boundary-element contexts for three-dimensional Helmholtz problems. In the particular case of the plane-wave scattering by a rigid sphere, errors obtained are consistent with some theoretical predictions given by de La Bourdonnaye (1994*a*, *b*) and Melenk & Babuška (1996). In practical terms, it has been found that 2.5–3 degrees of freedom per wavelength are sufficient to get satisfying results even for non-convex geometries. Since this addresses the most important factor limiting the use of discrete numerical methods in analysis of wave problems, this advance is expected to have significant impact on a wide variety of engineering simulations. At this stage, the two major limitations of the method are the time taken for the calculation of the system matrix and ill-conditioning problems associated with this new basis. These will be subject to further studies.

The authors are grateful for the support of the Engineering and Physical Sciences Research Council (EPSRC), for this work, through grant numbers GR/N09879, GR/K81652 and GR/M41025. We are also grateful to BAE SYSTEMS and particularly Dr David Rowse and Dr Simon Benham for their support and interest. P.B. is grateful to the EPSRC Senior Research Fellowship committee, chaired by Professor Sir Richard Brook, which is funding this work, through EPSRC grant number SF/000169.

References

Abboud, T., Nédélec, J.-C. & Zhou, B. 1995 Improvement of the integral equation method for high frequency problems. In *Proc. 3rd Int. Conf. on Mathematical Aspects of Wave Propagation Phenomena, SIAM, Philadelphia, PA, USA, 1995*, pp. 178–187. Philadelphia, PA: SIAM.

Babuška, I. & Melenk, J. M. 1997 The partition of unity method. *Int. J. Numer. Meth. Engng* **40**, 727–758.

Bayliss, A., Gunburger, M. & Turkel, E. 1992 Boundary conditions for the numerical solution of elliptic equations in exterior regions. *SIAM J. Appl. Math.* **42**, 430–451.

Bettess, P. 2004 Short-wave scattering: problems and techniques. *Phil. Trans. R. Soc. Lond.* A **362**, 421–443.

Bettess, P., Shirron, J., Laghrouche, O., Peseux, B., Sugimoto, R. & Trevelyan, J. 2003 A numerical integration scheme for special finite elements for Helmholtz equation. *Int. J. Numer. Meth. Engng* **56**, 531–552.

Cessenat, O. & Després, B. 1998 Application of an ultra weak variational formulation of elliptic PDEs to the two-dimensional Helmholtz problem. *SIAM J. Numer. Analysis* **35**, 255–299.

Cheung, Y. K., Jin, W. G. & Zienkiewicz, O. C. 1991 Solution of Helmholtz equation by Trefftz method. *Int. J. Num. Meth. Eng.* **32**, 63–78.

Darrigrand, E. 2002 Coupling of fast multipole method and microlocal discretization for the 3-D Hemholtz equation. *J. Computat. Phys.* **181**, 126–154.

de La Bourdonnaye, A. 1994*a* High frequency approximation of integral equations modelizing scattering phenomena. *Model. Math. Analyse Num.* **28**, 223–241.

de La Bourdonnaye, A. 1994*b* Une méthode de discrétisation microlocale et son application à un problème de diffraction. *C. R. Acad. Sci. Paris Sér. I* **318**, 385–388.

Després, B. 1994 Sur une formulation variationnelle de type ultra-faible. *C. R. Acad. Sci. Paris Sér. I* **318**, 939–944.

Duffy, M. G. 1982 Quadrature over a pyramide or cube with a singularity at a vertex. *SIAM J. Numer. Analysis* **19**, 1260–1262.

Farhat, C., Harari, I. & Franca, L. 2001 The discontinuous enrichment method. *Comput. Meth. Appl. Mech. Engng* **190**, 6455–6479.

Grannell, J. J., Shirron, J. J. & Couchman, L. S. 1994 A hierarchic *p*-version boundary-element method for axisymmetric acoustic scattering and radiation. *J. Acoust. Soc. Am.* **95**, 2320–2329.

Huttunen, T., Monk, P. & Kaipio, J. P. 2002 Computational aspects of the ultra weak variational formulation. *J. Computat. Phys.* **182**, 27–46.

Ihlenburg, F. & Babuška, I. 1995 Finite element solution to the Helmholtz equation with high wave number. I. The *h*-*p*-version of the FEM. *Comput. Meth. Appl. Mech. Engng* **30**, 9–37.

Ihlenburg, F. & Babuška, I. 1997 Finite element solution to the Helmholtz equation with high wave number. II. The *h*-version of the FEM. *SIAM J. Numer. Analysis* **34**, 315–358.

Kane, J. H. 1994 *Boundary element analysis in engineering continuum mechanics.* Englewood Cliffs, NJ: Prentice Hall.

Krommer, A. R. & Ueberhuber, C. W. 1998 *Computational integration.* Philadelphia, PA: SIAM.

Laghrouche, O. & Bettess, P. 2000 Short wave modelling using special finite elements. *J. Comput. Acoust.* **8**, 189–210.

Laghrouche, O., Bettess, P. & Astley, R. J. 2002 Modelling of short wave diffraction problems using approximating systems of plane waves. *Int. J. Numer. Meth. Engng* **54**, 1501–1533.

Lyness, J. N. & Jespersen, D. 1975 Moderate degree symmetric quadrature rules for the triangle. *J. Inst. Math. Applic.* **15**, 19–32.

Mayer, P. & Mandel, J. 1997 The finite ray element method for the Helmholtz equation of scattering: first numerical experiments. UCD/CCM report no. 111. University of Colorado, Boulder, CO, USA.

Melenk, J. M. & Babuška, I. 1996 The partition of unity finite element method: basic theory and applications. *Comput. Meth. Appl. Mech. Engng* **136**, 289–314.

Monk, P. & Wang, D.-Q. 1999 A least-squares method for the Helmholtz equation. *Comput. Meth. Appl. Mech. Engng* **175**, 121–136.

Morse, P. M. & Feshbach, H. 1953 *Methods of theoretical physics.* McGraw-Hill.

Ortiz, P. & Sanchez, E. 2001 An improved partition of unity finite element model for diffraction problems. *Int. J. Numer. Meth. Engng* **50**, 2727–2740.

Perrey-Debain, E., Trevelyan, J. & Bettess, P. 2003*a* Plane wave interpolation in direct collocation boundary element method for radiation and wave scattering: numerical aspects and applications. *J. Sound Vib.* **261**, 259–268.

Perrey-Debain, E., Trevelyan, J. & Bettess, P. 2003*b* Use of wave boundary elements for acoustic computations. *J. Comput. Acoust.* **11**, 305–321.

Perrey-Debain, E., Trevelyan, J. & Bettess, P. 2003*c* Plane wave basis in integral equations for 3D scattering. In *Proc. 6th Int. Conf. on Mathematical and Numerical Aspects of Wave Propagation, Finland, 2003*, pp. 292–297. Springer.

Schenck, H. A. 1968 Improved integral formulation for acoustic radiation problems. *J. Acoust. Soc. Am.* **44**, 41–58.

Stojek, M. 1998 Least-squares Trefftz-type elements for the Helmholtz equation. *Int. J. Numer. Meth. Engng* **41**, 831–849.